AIAA JOURNAL
Vol. 30, No. 7, July 1992

Validation of Finite Difference Boundary Condition Models for Solid Mechanics Applications

J. O. Dow* and J. L. Hardaway†
University of Colorado, Boulder, Colorado 80309

Five basic finite difference boundary condition models are validated using a process that embeds the boundary conditions in a larger problem with a known solution. The boundary conditions validated are: 1) fixed boundaries, 2) straight boundaries, 3) 90 deg re-entrant (concave) corners, 4) 90-deg outside (convex) corners, and 5) curved boundaries. The development depends on the use of a physically based notation that specializes the finite difference method for elasticity applications. The validation procedure can be extended to other boundary conditions. Five example problems are solved.

I. Introduction

RECENTLY, the finite difference method has been specialized for applications in solid mechanics.[1,2] The specialization is accomplished through the use of a physically based notation that directly relates the displacements in the continuum to the sources of these displacements; namely rigid body motions and strain quantities.[3,4] The use of this notation has allowed the development of straightforward, physically intuitive procedures for refining finite difference meshes[5,6] and for modeling complex boundaries between regions of different materials.[7]

The boundary models for the multimaterial interfaces are validated in the following way. First, a rectangular region consisting of a single material with fixed boundaries is solved for an arbitrary load using the finite difference method. This solution is considered to be correct because of the simplicity of the boundary conditions. Then the region is divided into two subregions. The boundary models are then applied to the appropriate subregion and this problem is solved. The boundary models used in the second analysis that reproduce the results of the equivalent portion of the larger problem are considered to accurately represent the boundary conditions.

The process described of validating boundary condition models by embedding them in a simple problem is used here to validate several standard representations of boundary conditions for plane elasticity problems. Specifically, the following boundary models are validated: 1) fixed boundaries, 2) straight boundaries, 3) 90-deg re-entrant (concave) corners, 4) 90-deg outside (convex) corners, and 5) curved boundaries.

The validation of these boundary condition models will extend the range of problems that can be solved confidently using the finite difference method. The boundary condition representations for coupled vector field problems as exemplified here by plane elasticity applications have not been previously validated. The treatment of boundary conditions for scalar problems does not extend directly to coupled vector field problems. With the validation of these boundary conditions, the finite difference method may become competitive with the finite element method in a variety of elasticity applications.

The next section presents the theoretical background required for the developments presented here. The third section defines the boundary condition representations being validated. These models are validated in the fourth section. The paper concludes with a summary and recommendations for further work.

II. Theoretical Background

The specialization of the finite difference method for elasticity applications is based on the use of strain gradient notation.[1,2] The fourth-order Taylor series expansions required to form the nine-node central difference templates utilized in most elasticity applications are given as:

$$
\begin{aligned}
u &= (u_{rb})_o + (\varepsilon_x)_o x + \left(\frac{\gamma_{xy}}{2} - r_{rb}\right)_o y \\
&\quad + \frac{1}{2}(\varepsilon_{x,x})_o x^2 + (\varepsilon_{x,y})_o xy \\
&\quad + \frac{1}{2}(\gamma_{xy,y} - \varepsilon_{y,x})_o y^2 + \frac{1}{2}(\varepsilon_{x,xy})_o x^2 y \\
&\quad + \frac{1}{2}(\varepsilon_{x,yy})_o xy^2 + \frac{1}{4}(\varepsilon_{x,xyy})_o x^2 y^2 \\
v &= (v_{rb})_o + \left(\frac{\gamma_{xy}}{2} + r_{rb}\right)_o x + (\varepsilon_y)_o y \\
&\quad + \frac{1}{2}(\gamma_{xy,x} - \varepsilon_{x,y})_o x^2 \\
&\quad + (\varepsilon_{y,x})_o xy + \frac{1}{2}(\varepsilon_{y,y})_o y^2 + \frac{1}{2}(\varepsilon_{y,xx})_o x^2 y \\
&\quad + \frac{1}{2}(\varepsilon_{y,xy})_o xy^2 + \frac{1}{4}(\varepsilon_{y,xxy})_o x^2 y^2
\end{aligned} \tag{1}
$$

These equations are expressed in local coordinates. The origin corresponds to the interior of the nine-node central difference template. The coefficients of these Taylor series expansions are expressed in terms of the physical quantities that produce displacements in the continuum. The rigid body terms u_{rb}, v_{rb}, and r_{rb} are considered zero-th order strain gradient quantities, while the constant strain terms ε_x, ε_y, and γ_{xy} are first-order terms. The higher order terms are exemplified by the second-order term $\gamma_{xy,x}$. This term quantifies the variation of γ_{xy} in the x direction. The subscript o on the strain gradient quantities indicates that these terms are Taylor series coefficients evaluated at the local origin.

The displacement representations given in Eq. (1) are used to form the finite difference operators. When the expressions

Received Aug. 8, 1991; revision received Nov. 6, 1991; accepted for publication Nov. 21, 1991.

*Associate Professor, Department of Civil, Environmental, and Architectural Engineering. Member AIAA.

†Graduate Research Assistant, Department of Civil, Environmental, and Architectural Engineering. Member AIAA.

for u and v are evaluated at the nine mesh points by substituting the appropriate nodal locations into Eq. (1), a set of 18 equations is formed. The inverse of this transformation produces the difference approximations represented by the nine-node central difference template as:

$$\{\varepsilon,\} = [\Phi]^{-1}\{u\} \tag{2}$$

where

$$\{u\} = \{u_1 v_1 u_2 v_2 u_3 v_3 u_4 v_4 u_5 v_5 u_6 v_6 u_7 v_7 u_8 v_8 u_9 v_9\}^T$$

$$\{\varepsilon,\} = \{u_{rb} v_{rb} r_{rb} \varepsilon_x \varepsilon_y \gamma_{xy} \varepsilon_{x,x} \varepsilon_{y,x} \gamma_{xy,x} \varepsilon_{x,y} \varepsilon_{y,y} \gamma_{xy,y} \varepsilon_{x,xy} \varepsilon_{x,yy} \varepsilon_{y,xy} \varepsilon_{y,xx} \varepsilon_{x,xyy} \varepsilon_{y,xxy}\}_o^T$$

The subscripts on the displacements refer to a point in the central difference template. The vector $\{\varepsilon,\}$ consists of the 18 strain gradient quantities contained in Eq. (1). These are the quantities approximated by the 3 × 3 central difference template. The inverse of $[\Phi]$ is the 18 × 18 matrix that defines the finite difference operators. For an evenly spaced mesh, the derivative approximations are identical to the standard finite difference operators. For example, the fourth row of Eq. (2) contains the difference approximation for the normal strain $\{\varepsilon_x\}$. Examples of the finite difference operators resulting from evenly spaced and distorted templates are given in Refs. 2 and 5.

The difference operators just formed are used to approximate the governing differential equations and to model the boundary conditions for plane stress problems. The equilibrium equations that govern the behavior of planes' stress problems are the following coupled second-order differential equations:

$$\left(\frac{E}{1-\nu^2}\right)\left[\frac{\partial^2 u}{\partial x^2} + \nu\frac{\partial^2 v}{\partial x \partial y} + \left(\frac{1-\nu}{2}\right)\left(\frac{\partial^2 u}{\partial x^2} + \frac{\partial^2 v}{\partial x \partial y}\right)\right] = -f_x$$

$$\left(\frac{E}{1-\nu^2}\right)\left[\frac{\partial^2 v}{\partial y^2} + \nu\frac{\partial^2 u}{\partial x \partial y} + \left(\frac{1-\nu}{2}\right)\left(\frac{\partial^2 v}{\partial x^2} + \frac{\partial^2 u}{\partial x \partial y}\right)\right] = -f_y \tag{3}$$

where f_x and f_y are the body forces in the x and y directions. The parameters E and ν are Young's modulus and Poisson's ratio. These equations can be rewritten in strain gradient notation as:

$$\varepsilon_{x,x} + \nu\varepsilon_{y,x} + \left(\frac{1-\nu}{E}\right)\gamma_{xy,y} = -\left(\frac{1-\nu^2}{E}\right)f_x$$

$$\varepsilon_{y,y} + \nu\varepsilon_{x,y} + \left(\frac{1-\nu}{E}\right)\gamma_{xy,x} = -\left(\frac{1-\nu^2}{E}\right)f_y \tag{4}$$

Inspection of the strain gradient quantities given in Eq. (2) by the vector $\{\varepsilon,\}$ shows that this vector contains the six strain gradient quantities contained in Eq. (4). Thus, the nine-node central difference template is capable of approximating the governing equations for plane elasticity. When the derivatives in the governing equations are replaced by the appropriate finite difference operators given in $[\Phi]^{-1}$, the result can be written symbolically as:[1,2]

$$[\Omega]\{u\} = -\{f\} \tag{5}$$

The two equations contained in Eq. (5) are approximations of the equilibrium equations in the x and y directions at the interior node of the central difference templates. The matrix $[\Omega]$ consists of a linear combination of the difference operators for the strain gradient terms contained in Eq. (4). The vector $\{f\}$ contains the two terms on the right-hand side of Eq. (4).

III. Finite Difference Boundary Condition Models

The finite difference boundary models validated in this work are defined in this section using strain gradient notation. The four distinct boundary condition models are formulated in turn.

A. Fixed Boundary

The fixed boundary is the simplest of the finite difference boundaries to model. The finite difference mesh for this sloping boundary is shown in Fig. 1. The displacements of the nodes on the boundary are specified to be zero. The finite difference approximation of a boundary value problem with fixed boundaries will not explicitly contain the boundary nodes because their displacements are known. Thus, there is no need to satisfy the approximations of the governing differential equations for the fixed nodes in the primary finite difference model in order to determine the approximate displacements for the problem.

As a result, the finite difference model of a boundary value problem with fixed boundaries is constructed by assembling the approximation of the governing differential equation given in Eq. (5) for each of the interior points.

$$[\Omega_s]\{u_s\} = -\{f_s\} \tag{6}$$

where the matrix $[\Omega_s]$ is the system coefficient matrix approximating the governing differential equations, the vector $\{u_s\}$ contains the unknown displacements, and the vector $\{f_s\}$ contains the body forces applied at each of the mesh points.

However, in many applications, the stresses and strains are the actual quantities sought from an analysis. These quantities can be found in the following way. The boundary is assumed to be free, as shown in Fig. 2. As a result of the initial assumption concerning the fixed boundary condition, the displacements of the boundary nodes are known to be zero. The displacements of the interior nodes are known as a result of solving the finite difference approximation of the boundary value problem. However, the displacements of the fictitious nodes shown in Fig. 2 are not known. These displacements can be found by solving a set of auxiliary equations that force the approximations of the partial differential equations to be satisfied on the boundary. The number of unknown displacements associated with the fictitious nodes is equal to the number of equations available from satisfying the approximation of the governing differential equations on the boundary.

Now that all of the displacements associated with the nine-node central difference template on the boundary are known, the boundary stresses and strains can be computed from the finite difference operator given in Eq. (2). The normal and

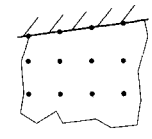

Fig. 1 Fixed boundary.

Fig. 2 Boundary with finite difference mesh.

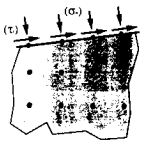

Fig. 3 Normal and tangential stresses on boundary.

tangential stresses on the boundary, as shown in Fig. 3, can be written in terms of the stresses in the global coordinate system as:

$$\begin{Bmatrix} \sigma_n \\ \tau_t \end{Bmatrix} = \begin{bmatrix} \cos^2\theta & \sin^2\theta & 2\sin\theta\cos\theta \\ -\sin\theta\cos\theta & \sin\theta\cos\theta & \cos^2\theta - \sin^2\theta \end{bmatrix} \begin{Bmatrix} \sigma_x \\ \sigma_y \\ \tau_{xy} \end{Bmatrix} \tag{7}$$

The stresses in the global system are related to the strains in the global system with the constitutive relation as:

$$\begin{Bmatrix} \sigma_x \\ \sigma_y \\ \tau_{xy} \end{Bmatrix} = \frac{E}{1-\nu^2} \begin{bmatrix} 1 & \nu & 0 \\ \nu & 1 & 0 \\ 0 & 0 & \dfrac{1-\nu}{2} \end{bmatrix} \begin{Bmatrix} \varepsilon_x \\ \varepsilon_y \\ \gamma_{xy} \end{Bmatrix} \tag{8}$$

The strains are approximated in terms of the nodal displacements using the differential operators for the three strain terms with the following equation:

$$\{\varepsilon\} = [D][\Phi]^{-1}\{u\} \tag{9}$$

where

$$[D] = \begin{bmatrix} 0&0&0&1&0&0&0&0&0&0&0&0&0&0&0&0&0&0 \\ 0&0&0&0&1&0&0&0&0&0&0&0&0&0&0&0&0&0 \\ 0&0&0&0&0&1&0&0&0&0&0&0&0&0&0&0&0&0 \end{bmatrix}$$

The matrix $[D]$ is used so the strains can be directly related to the differential operators given in Eq. (2). This matrix selects the appropriate strain approximations from the finite difference operators.

This section has outlined the characteristics of a fixed boundary. The displacements on the boundary are known to be zero and the approximations of the governing differential equations must be satisfied. By explicitly satisfying the approximations of the differential equations, the displacements of the fictitious nodes shown in Fig. 2 can be found. When the quantities are known, the boundary stresses can be computed by substituting the known displacements into Eqs. (7–9). It should be noted that this analysis is applicable to the case where the boundary is given an initial displacement other than zero.

B. Loaded Boundary

A boundary with applied loads is identical in concept to the fixed boundary except that the quantities known at the start of the analyses differ. In a fixed boundary condition, the displacements on the boundary are known and the stresses must be found. In the case of a loaded boundary, the normal and tangential stresses are known and the boundary displacements must be found. In many problems, the loads on the boundary are zero

A loaded boundary is included in the finite difference model in the following way. The approximations of the governing differential equations given by Eq. (5) must be satisfied at each point in the interior and on the boundary. The nine-node central difference templates associated with the boundary points introduce the fictitious points as shown in Fig. 2 into the problem formulations as unknowns. Each of the fictitious points introduces two unknown displacements into the model. Thus, two equations must be added to the set of equations provided by satisfying Eq. 5 at each interior and boundary point so that the number of equations equals the number of unknowns. In fact, the fictitious nodes can be seen as a guide that dictates the number of auxiliary equations that are required to complete the finite difference model.

These extra equations are provided by introducing the boundary loads in terms of the normal and tangential stresses. The normal and tangential stresses, as given by Eq. (7), are transformed to a function of mesh point displacements with Eqs. (8) and (9). When the boundary loads for each of the boundary points are assembled, the result is

$$[\Omega_b]\{u_s\} = -\{f_b\} \tag{10}$$

where the matrix $[\Omega_b]$ is the system coefficient matrix introducing the boundary loads, the vector $\{u_s\}$ contains the unknown displacements including the fictitious nodes, and the vector $\{f_b\}$ contains the boundary loads. The same analysis applies to curved boundaries. Both straight and curved boundary models are validated in the next section.

Equations (6) and (10) can be combined to give the complete finite difference model for a boundary value problem with the loaded boundaries as:

$$\begin{bmatrix} \Omega_s & 0 \\ 0 & \Omega_b \end{bmatrix} \{u_s\} = \begin{Bmatrix} -f_s \\ f_b \end{Bmatrix} \tag{11}$$

The procedure just discussed produces a set of $2n$ equations where n is the number of interior and fictitious points. Often for the sake of compactness, the size of the final set of equations is reduced to $2n$ where n does not include the fictitious nodes. This is accomplished by partitioning Eq. (10) as follows:

$$[\Omega_{bd} \mid \Omega_{bf}] \begin{Bmatrix} u_{sd} \\ u_{sf} \end{Bmatrix} = \{f_b\} \tag{12}$$

where the vector $\{u_{sd}\}$ represents the displacements on the boundary and in the domain and the vector $\{u_{sf}\}$ represents the displacements of the fictitious nodes. This equation can be solved for the displacements of the fictitious nodes to give

$$\{u_{sf}\} = \{f_b\} - [\Omega_{bf}]^{-1}[\Omega_{bd}]\{u_{sd}\} \tag{13}$$

Equation (13) allows the overall size of the problem to be reduced by eliminating the fictitious nodes from Eq. (6).

C. Loaded Re-entrant Corner

A re-entrant corner and the finite difference mesh associated with it are shown in Fig. 4. In principle, the re-entrant corner is treated exactly like a straight boundary. The only question to be answered concerns the fictitious node shown in solid black in Fig. 4. There are three choices of normal and tangential stresses that could be associated logically with this node. The first two are the stresses at the points on the boundary connected to the fictitious node with dashed lines. The third choice is to associate the stresses at the boundary point in the corner with the fictitious point. Although all three of these options are found to be satisfactory models, the third option will be recommended as the most representative model with the following argument.

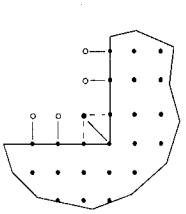

Fig. 4 Re-entrant corner with finite difference mesh.

A typical set of boundary loads is shown in Fig. 5. The normal stresses σ_x and σ_y are shown in Figs. 5a and 5b. The shear stresses on the two surfaces are shown in Figs. 5c and 5d. The boundary stresses in the corner are introduced into the model using Eqs. (7–9). The transformation angle used in Eq. (7) is shown in Fig. 4 by the solid line to the fictitious node. The use of this approach allows values for σ_x, σ_y, and τ_{xy} to be introduced into the model. If either of the other two options is used, only two of these values will be included in the representation. It is recommended that the average value of the shear stresses on the two surfaces be used for the value of τ_{xy}.

When the boundary condition models for each of the boundary points are assembled, the auxiliary equations have the same form as Eq. (10). The final form of a finite difference model containing loaded boundaries with re-entrant corners has the form of Eq. (11).

D. Loaded Corner

A convex corner and the associated finite difference mesh are shown in Fig. 6. This corner presents the opposite problem encountered in the case of the re-entrant corner. In the re-entrant corner, there were three possibilities for incorporating the one fictitious node at the corner into the finite difference model. Here there are three fictitious nodes at the corner that must be included in the finite difference model and only one boundary point that is associated with these three points.

This problem has been treated previously using strain gradient notation.[2] In this earlier treatment, a reduced central difference template was used. The results compared well with finite element results, so this approach is acceptable. However, this reduced template approach did not prove satisfactory in representing multimaterial problems,[7] so an alternative approach was developed to represent both problems.

In order to account for the six displacements associated with the three fictitious nodes, six auxiliary equations must be specified. To be useful, the six auxiliary conditions must be available from the known boundary loads. The normal and shear stresses applied to the boundary are shown in Figs. 7a and Fig. 7b, respectively. These loading conditions allow the following stress quantities to be specified at the corner node: σ_n, τ_t, $\sigma_{x,y}$, $\sigma_{y,x}$, $\tau_{xy,x}$, $\tau_{xy,y}$.

The first two quantities are immediately apparent. These are the normal and tangential stresses at the corner. The line

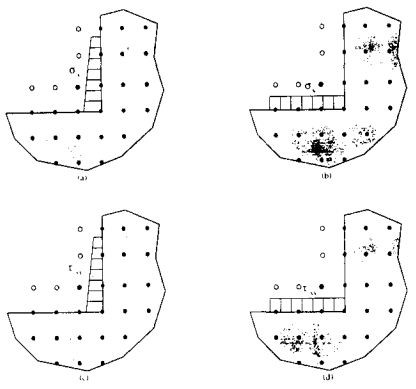

Fig. 5 Boundary loads on a re-entrant corner: a) normal stress $\{\sigma_x\}$; b) normal stress $\{\sigma_y\}$; c) shear stress $\{\tau_{xy}\}$; d) shear stress $\{\tau_{xy}\}$

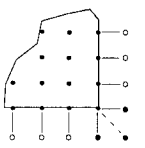

Fig. 6 Convex corner with finite difference mesh.

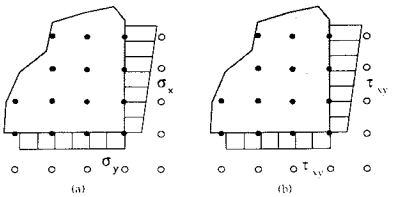

Fig. 7 Boundary loads on convex corner: a) normal stresses; b) shear stresses.

normal to the corner is shown as the dashed line in Fig. 6. The next two quantities are gradients of the normal stresses σ_x and σ_y. The value of these quantities can be computed from the stress values shown in Fig. 7a. For example, $\sigma_{y,x}$ is the rate of change of σ_y in the x direction shown in Fig. 7a. For the loading condition shown, the normal stress σ_y is constant therefore $\sigma_{y,x}$ is equal to zero. However, σ_x is not constant in Fig. 7a, so $\sigma_{x,y}$ has a negative value because σ_x decreases as y increases. Similarly values for $\tau_{xy,x}$ and $\tau_{xy,y}$ are available from Fig. 7b. In this case, $\tau_{xy,x}$ is negative and $\tau_{xy,y}$ is zero. These quantities allow the fictitious nodes to be included in the analysis using boundary loads that are normally known.

The auxiliary equations associated with σ_n and τ_t are included in the analysis through the use of Eq. (7). Equations (8) and (9) are used to incorporate the fictitious nodes. The stress gradient quantities are incorporated in the analysis by taking the derivatives of Eq. (8). For example, when the derivative of Eq. (8) with respect to x is taken, the result is

$$\begin{Bmatrix} \sigma_{x,x} \\ \sigma_{y,x} \\ \tau_{xy,x} \end{Bmatrix} = \frac{E}{1-\nu^2} \begin{bmatrix} 1 & \nu & 0 \\ \nu & 1 & 0 \\ 0 & 0 & \dfrac{1-\nu}{2} \end{bmatrix} \begin{Bmatrix} \varepsilon_{x,x} \\ \varepsilon_{y,x} \\ \gamma_{xy,x} \end{Bmatrix} \tag{14}$$

In this case only $\sigma_{y,x}$ and $\tau_{xy,x}$ are used as auxiliary equations.

The quantities on the right-hand side of Eq. (14) are available from the finite difference operator given in Eq. (2). The specific strain gradient quantities desired are extracted with a relation similar to Eq. (9). The only difference is that the $[D]$ matrix becomes

$$[D] = \begin{bmatrix} 0&0&0&0&0&0&1&0&0&0&0&0&0&0&0&0&0&0 \\ 0&0&0&0&0&0&0&1&0&0&0&0&0&0&0&0&0&0 \\ 0&0&0&0&0&0&0&0&1&0&0&0&0&0&0&0&0&0 \end{bmatrix}$$

This matrix extracts the strain gradient terms on the right-hand side of Eq. (14) from the finite difference operator given by Eq. (2).

A similar process is available for the strain gradients in the y direction. In this case, the stress gradients in the y direction are given as:

$$\begin{Bmatrix} \sigma_{x,y} \\ \sigma_{y,y} \\ \tau_{xy,y} \end{Bmatrix} = \frac{E}{1-\nu^2} \begin{bmatrix} 1 & \nu & 0 \\ \nu & 1 & 0 \\ 0 & 0 & \dfrac{1-\nu}{2} \end{bmatrix} \begin{Bmatrix} \varepsilon_{x,y} \\ \varepsilon_{y,y} \\ \gamma_{xy,y} \end{Bmatrix} \tag{15}$$

In this case only $\sigma_{y,y}$ and $\tau_{xy,y}$ are used. The corresponding $[D]$ matrix is the following:

$$[D] = \begin{bmatrix} 0&0&0&0&0&0&0&0&0&1&0&0&0&0&0&0&0&0 \\ 0&0&0&0&0&0&0&0&0&0&1&0&0&0&0&0&0&0 \\ 0&0&0&0&0&0&0&0&0&0&0&1&0&0&0&0&0&0 \end{bmatrix}$$

This matrix extracts the strain gradient terms on the right hand side of Eq. (15) from the finite difference operator given by Eq. (2).

When the auxiliary equations for all of the boundary points are assembled, they have the same form as Eq. (10). The

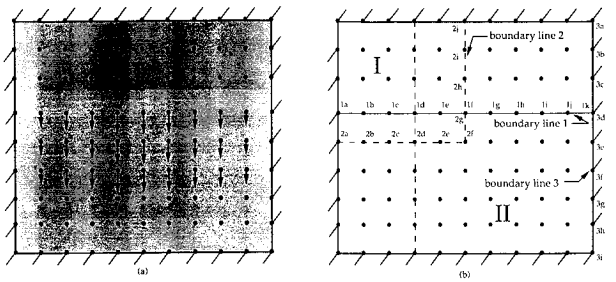

Fig. 8 Example problem: a) applied loads; b) interface lines.

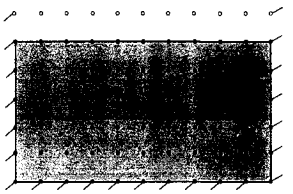

Fig. 9 Lower section of example problem.

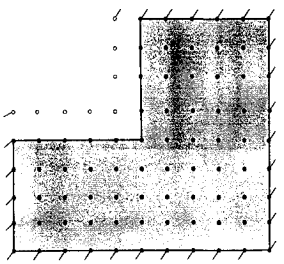

Fig. 10 Re-entrant corner section of example problem.

final structure of a finite difference representation containing a convex corner is identical to the previous representations.

IV. Boundary Condition Model Validation

The boundary models just developed are now validated. This is accomplished by embedding a smaller problem containing these models in a larger problem with a known solution. If the results of the small problem explicitly containing the boundary model match those of the larger problem, the boundary model is a good representation of the boundary condition. The boundary condition models are embedded in the control problem shown in Fig. 8a. The control problem consists of a rectangular region with fixed boundaries. The applied load is centered and varies as shown. The arrows attached to the nodes are proportional to the distributed load. The mesh point separation is five units.

The loaded boundary discussed in Section IIIB. is validated first. The displacements are found for the full region shown in Fig. 8a. Then the stresses on boundary line 1 are computed. The displacements and stresses at the mesh points on this line are given in Table 1. The lower section of the region shown in Fig. 8b is modeled as the separate problem shown in Fig. 9. The stresses σ_y and τ_{xy} found for the full problem contained in Table 1, are applied to the free boundary of the smaller problem as normal and tangential boundary loads. When the reduced problem is solved using the boundary condition model developed in Sec. IIIB, the displacement and strain results match those for the corresponding portion of the larger problem. The boundary displacements and stresses are identical to those given in Table 1. The fact that the results of the torting a mesh are given in Ref. 2. However, a distorted mesh need not be utilized to represent this problem accurately. The boundary stresses can be applied to points on the continuum model explicitly containing the boundary model are identical to those found from the larger problem shows that the boundary model for loaded straight edges accurately represents the boundary condition.

The loaded corner models developed in Secs. IIIC and IIID are now validated. The problem shown in Fig. 8 is used again in the validation. The displacements and stresses computed for the nodes on boundary line 2 are presented in Table 2. The larger portion of the region separated by boundary line 2 contains a re-entrant corner, as shown in Fig. 10. This subregion is modeled as a separate problem. The boundary stresses found for the full problem as given in Table 2 are applied to the subregion according to the model developed in Section IIIC. The displacements and strains produced by this analysis match the corresponding quantities found for the control problem. Thus, the model developed in Sec. IIIC correctly represents the re-entrant corner. A similar analysis is performed for the complimentary region containing the convex corner. The analysis produces the desired results, therefore the model developed in Section IIID correctly represents the convex corner.

The model developed in Sec. IIIB will now be applied to a curved boundary. The boundary model being validated is embedded in the problem shown in Fig. 11a. An arbitrary load is applied along the top and bottom of the region, as shown. It should be noted that this mesh is not regular. Some of the mesh points in the interior have been moved so they lie on the boundary of the circular section being removed from the rectangular region to test the boundary model. The curved boundary being modeled is shown in Fig. 11b. When the stresses generated in the problem of Fig. 11a are applied to the problem shown in Fig. 11b as boundary loads, the corresponding displacements and strains in the two problems are identical. Thus, the boundary model developed in Sec. IIIB successfully represents curved boundaries.

The model just described utilized a distorted mesh to represent the interior boundary. The formulation of the finite difference operators for distorted meshes is identical to the process discussed in Sec. II. Examples of the effects of dis-

Table 1 Displacements and stresses: boundary line 1

	Displacements		Stresses		
Node	u	v	σ_x	σ_y	τ_{xy}
1a	0.000	0.000	45.281	13.584	−63.398
1b	0.014	−0.005	87.200	87.641	−128.513
1c	0.020	−0.013	79.669	203.435	−123.144
1d	0.020	−0.019	60.855	278.951	−114.543
1e	0.013	−0.026	59.327	397.236	−80.766
1f	0.000	−0.028	51.063	424.063	0.000
1g	−0.013	−0.026	59.327	397.236	−80.766
1h	−0.020	−0.019	60.855	278.951	−114.543
1i	−0.020	−0.013	79.669	203.435	−123.144
1j	−0.014	−0.005	87.200	87.641	−128.513
1k	0.000	0.000	45.281	13.584	−63.398

Table 2 Displacements and stresses: boundary line 2

	Displacements		Stresses		
Nodal	u	v	σ_x	σ_y	τ_{xy}
2a	0.000	0.000	0.000	0.000	−69.244
2b	0.000	−0.006	0.000	0.000	−136.950
2c	0.000	−0.015	0.000	0.000	−129.985
2d	0.000	−0.021	0.000	0.000	−121.060
2e	0.000	−0.029	0.000	0.000	−86.597
2f	0.000	−0.031	0.000	0.000	0.000
2g	0.000	−0.028	51.063	424.063	0.000
2h	0.000	−0.018	74.657	609.007	0.000
2i	0.000	−0.008	85.724	557.214	0.000
2j	0.000	0.000	82.767	275.895	0.000

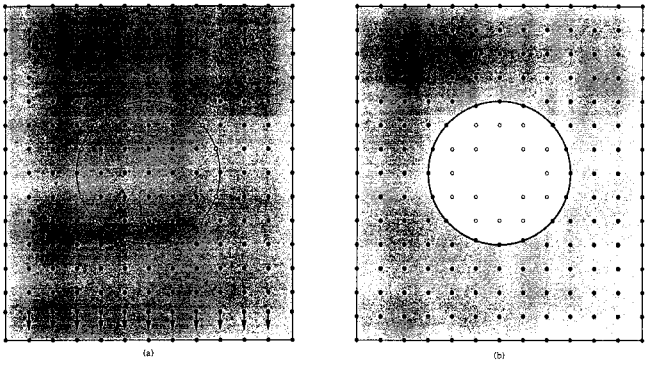

Fig. 11 Embedded circle example problem: a) applied loads; b) circular hole with fictitious nodes.

Table 3 Displacements and stresses: boundary line 3

	Displacements		Stresses		
Nodal	u	v	σ_x	σ_y	τ_{xy}
3a	0.000	0.000	0.000	0.000	0.000
3b	0.000	0.000	54.234	16.270	25.425
3c	0.000	0.000	66.480	19.944	45.597
3d	0.000	0.000	45.281	13.584	63.398
3e	0.000	0.000	0.000	0.000	69.244
3f	0.000	0.000	−45.281	−13.584	63.398
3g	0.000	0.000	−66.480	−19.944	45.597
3h	0.000	0.000	−54.234	−16.270	25.425
3i	0.000	0.000	0.000	0.000	0.000

that are not mesh points. This capability is made possible by including higher order Taylor series terms in the expression for the boundary loads given in Eq. (9). The problem just solved with a distorted mesh was also solved with an even mesh. This model also validated the boundary condition representation.

Finally, the boundary model for the fixed boundary developed in Sec. IIIA will be validated. The problem shown in Fig. 8 is used again in the validation. The stresses computed on the fixed boundary line 3 are applied as boundary loads to this boundary when it is unrestrained. When this problem is solved, the boundary displacements are found to be zero and the σ_x stresses match those originally found. The original fixed boundary displacements are obviously zero; thus, the boundary model discussed in Sec. IIIA is correct.

Conclusion

The work presented here has validated the boundary models for a set of frequently used boundary conditions. The procedure discussed in Sec. IIIA for finding reaction stresses on a fixed boundary provides the basis for modeling the other boundary conditions. The loaded straight boundary discussed in Sec. IIIB was presented largely for completeness. It should be noted that the formulation of the finite difference operators given by Eq. (2) is not restricted to regular meshes, so this boundary model also applies to boundaries that slope with respect to the global coordinate system. This contention is validated by the solution of the problem containing the circular hole. The boundary models developed here for the concave and convex corners are the results that have the most immediate usefulness. The clear definition of the boundary models in terms of the applied loads allows analysts to represent corners in finite difference models with confidence. However, the most valuable contribution of this work is likely to be the procedure used here to validate the boundary conditions. The process of embedding a boundary condition in a larger problem is applicable to boundary conditions other than those presented here. The availability of this process allows other boundary condition models to be validated as they are required. This will assist the finite difference method to become more useful in solid mechanics applications.

References

[1]Dow, J. O., Jones, M. S., and Harwood, S. A., "A Generalized Finite Difference Method for Solid Mechanics," *Numerical Methods for Partial Differential Equations*, Vol. 6, No. 2, 1990, pp. 137–152.

[2]Dow, J. O., Jones, M. S., and Harwood, S. A., "A New Approach to Boundary Modeling for Finite Difference Applications in Solid Mechanics," *International Journal for Numerical Methods in Engineering*, Vol. 30, No. 1, 1990, pp. 99–113.

[3]Dow, J. O., Feng, C. C., and Bodley, C. S., "An Equivalent Continuum Representation of Structures Composed of Repeated Elements," *AIAA Journal*, Vol. 23, No. 10, 1985, pp. 1564–1569.

[4]Dow, J. O., and Huyer, S. A., "Continuum Models of Space Station Structures," *Journal of Aerospace Engineering*, Vol. 2, No. 4, 1989, pp. 212–230.

[5]Stevenson, I., "A Generalized Adaptive Refinement Procedure for Finite Element and Finite Difference Analyses," Masters Thesis, Univ. of Colorado, 1990.

[6]Dow, J. O., and Stevenson, I., "An Adaptive Refinement Procedure for the Finite Difference Method," *Numerical Methods for Partial Differential Equations*, Vol. 8, No. 6, 1992, pp. 622–630.

[7]Dow, J. O., and Hardaway, J. L., "The Modeling of Multi-Material Interfaces in the Finite Difference Method," *Numerical Methods for Partial Differential Equations*, Vol. 8, No. 5, 1992, pp. 510–517.